Greener Journal of Geology and Earth Sciences

ISSN: 2354-2268

Submitted: 17/02/2016
Accepted: 27/02/2016
Published: 30/05/2016

DOI: http://doi.org/10.15580/GJGES.2016.1.021716041

Geology and Radioactivity of the Basement Rocks of Wadi El-Sahu Area, Southwestern Sinai, Egypt

By

El Mezayen AM
Abu Bakr MA
Sherif HMY
El Nahas HA
Ali HH

Research Article (DOI: http://doi.org/10.15580/GJGES.2016.1.021716041)

Geology and Radioactivity of the Basement Rocks of Wadi El-Sahu Area, Southwestern Sinai, Egypt

El Mezayen AM[1]*, Abu Bakr MA[2], Sherif HMY[2], El Nahas HA[2] and Ali HH[1]

[1]El Azhar University, Egypt.
[2]Nuclear Materials Authority, Cairo, Egypt.

*Corresponding Author's Email: aelmezayen50@ hotmail. com

ABSTRACT

The study area is covered by basement and sedimentary rocks. The basement rocks are represented by paragneiss, orthogneiss and younger granites, while the sedimentary succession is represented by clastic Paleozoic rocks. The younger granites are microscopically distinguished into monzogranite and syenogranite. Geochemically, the studied younger granites are peraluminous with alkaline affinity (moderately alkaline) originated in extensional regime. Monzogranite belongs to I-type granite formed in volcanic arc tectonic setting, while the syenogranite belongs to A-type formed in within-plate tectonic setting. The studied gneisses are nearly non-radioactive, whereas the studied younger granites are moderately radioactive where monzogranite is relatively higher than the syenogranite. The radio elements of these younger granites are incorporated in their accessory minerals such as zircon, xenotime and allanite. An anomalous quartz vein containing deep violet fluorite and kasolite is recorded cross-cutting the younger granites.

Keywords: Basement rock, Sedimentary rock, Monzogranite, Syenogranite, Uranium potential.

INTRODUCTION

Wadi El Sahu area is located in the southern part of Sinai Peninsula east of Abu Zeneima Town at distance of about 30 km and occupies approximately260 km^2. It is delineated by Longitudes 33^o 20′and 33^o 28′ E and Latitudes 28^o 52′ and 29^o 00′ N(Fig. 1).

A relatively few studies were carried out on the basement rocks outcropped at Wadi El Sahu and the surrounding areas. The younger granites of southwestern Sinai are generally classified into monzo and syenogranites (Azzaz, 1993; Abdel-Karim, 1996; Hassan, 1997; Sherif, 1998; Bishr, 2003; and Gabr, 2005).

Hassan (1997) mentioned that, the younger granites of Wadi El Shallal have alkaline to calc-alkaline, peraluminous to slightly metaluminous affinities, emplaced under syn-collision regime and belong to S-type granites.

Sherif (1998) studied the geology and uranium potentiality of the exposed basement rocks of Wadi Seih area southwestern Sinai. He classified the younger granites, according to their field relationships, into three varieties; the first is medium to coarse grained with pinkish white color, the second is medium grained with red color and it is mildy weathered and the third is porphyritic, fine to medium grained with red color. He concluded that, the radiometric anomalies are generally concentrated in the first and third varieties of the younger granites and the associated pegmatites. He added that, these anomalies are lithologically and structurally controlled.

Sherif and Ragab, (2004) studied the gneisses that exposed at Wadi Abu El Tiyour and stated that they are represented by garnet-biotite gneiss, while the gneisses that exposed around Wadi Seih are represented by biotite-hornblende gneiss as stated by Sherif, (1998).

El Husseiny (2008) studied the younger granites of Wadi El Sahu- Wadi El Seih area and classified them as monzogranite with fluorite, zircon, apatite, allanite and monazite as accessory minerals. Geochemically, it is highly fractionated; originated from non-alkaline magma similar to A-type granites and developed in post-orogenic tectonic environment.

Geologic Setting

A geologic map of the studied area modified after Bishr, (2003),(Fig. 1). The area is covered with basement and sedimentary rocks. The basement rocks are represented by gneisses and younger granites, while the sedimentary succession is represented by clastic Paleozoic rocks.

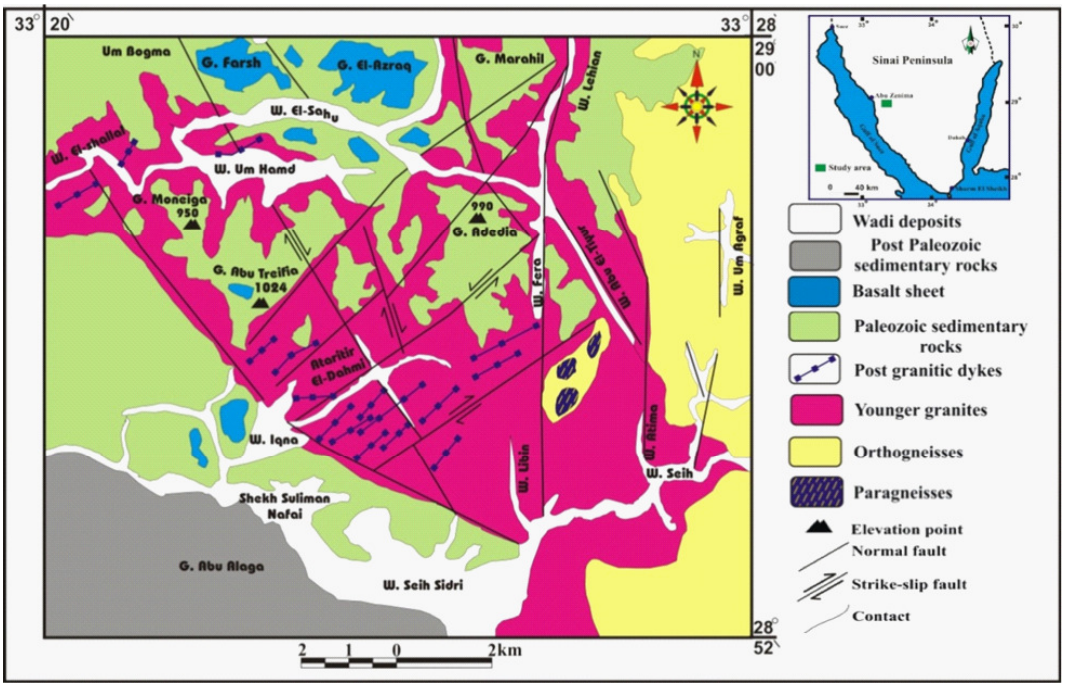

Figure 1: Location and geologic maps of Wadi El Sahu area, modified after Bishr, (2003).

Gneisses

The gneiss rocks are outcropping in the eastern side of the mapped area especially at Wadi Abu El Tiyour and Wadi Fera. These exposed gneisses are mainly paragneiss and orthogniess. These rocks are gray to whitish gray in color, medium to coarse grain, moderately weathered and show moderate to high relief. They are intensively folded and exhibit gneissose structure in which melanocratic and leucocratic bands are alternated (Fig. 2A). Sedimentary bedding is still preserved as characteristic feature for the studied paragniess (Fig. 2B)

The studied gneissis affected by tectonic processes which resulted in normal faults that strike in NNW-SSE, NNE-SSW and N-S directions and dissected by post-granitic dykes trending NNE-SSW to NE-SW (Hassan, 1997).

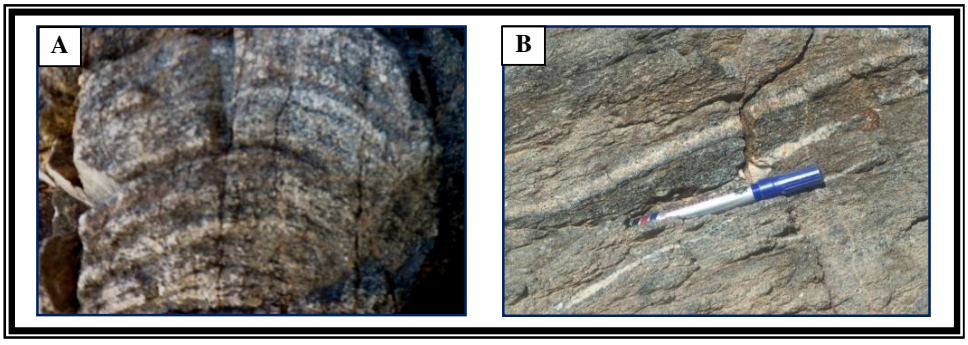

Figure 2: Photographs showing field description for the studies gniesses.
A- Well-developed gneissose structure and microanticlinal fold.
B- Well preserved sedimentary bedding.

Younger Granites

The younger granites are the most predominant rock unitexposed in the studied area. They are exposed mainly in the central and southwestern parts of the mapped area and dissected by many wadis such as Wadi El Shallal, Wadi Um Hamad and Wadi Fera. According to field investigations and microscopic examinations, the studied younger granites are differentiated into two types; monzogranite and syenogranite, which are corresponding to phase III granites (true granites) proposed by Sabet et al., (1976) and Abu El Leil (1980) . The contact between

the two granitic types is gradational. This contact is generally suggesting their derivation from the same magmatic source by differentiation processes.

The younger granites of the studied area show very high relief mountains. They are intruded into the gneisses with sharp intrusive contacts and sometimes occur as apophyses in the gneiss rocks (Fig.3A). The studied younger granites are unconformably overlain by Paleozoic sedimentary rocks (Fig. 3B). They are medium to coarse grained with pinkish white color, altered, highly jointed, sheared and show cavernous weathering (Fig. 3C).

The studied younger granites contain pegmatite bodies which occur either as elongated or subrounded bodies (Fig 3D). Sometimes, the younger granites are marked by the presence of parallel NE-SW trending fluorite-bearing quartz vein (Fig. 3E) as indicated by the presence of deep violet fluorite, hematitization and silicification. The radioactivity along this vein is high due to the presence of kasolite, Bishr, (2003). The studied granites are dissected by several normal faults (N-S, NNW-SSE and NW-SE trends) as well as strike-slip faults (NW-SE and NE-SW trends), Hassan, (1997).

Post Granitic Dykes

The above mentioned basement rock types are traversed by different dykes which occur either as swarms (Fig. 3F) or as single dykes. Hassan, (1997) and Bishr, (2003) described the post-granitic dykes of Wadi El Sahu as basalt, andesite, bostonite, rhyodacite, rhyolite and microgranite. Bishr (2003) stated "presence of high radioactive intensities associated with the zone of intersection of two basic dykes cross-cutting the younger granite of Wadi Um Hamad". He suggests that, the enrichment of uranium is occurred by secondary processes where the leachable uranium from the granite could be trapped or precipitated by the alteration products such as kaolinite and iron oxides, which observed along the fractures of the basic dykes and their intersection zone.

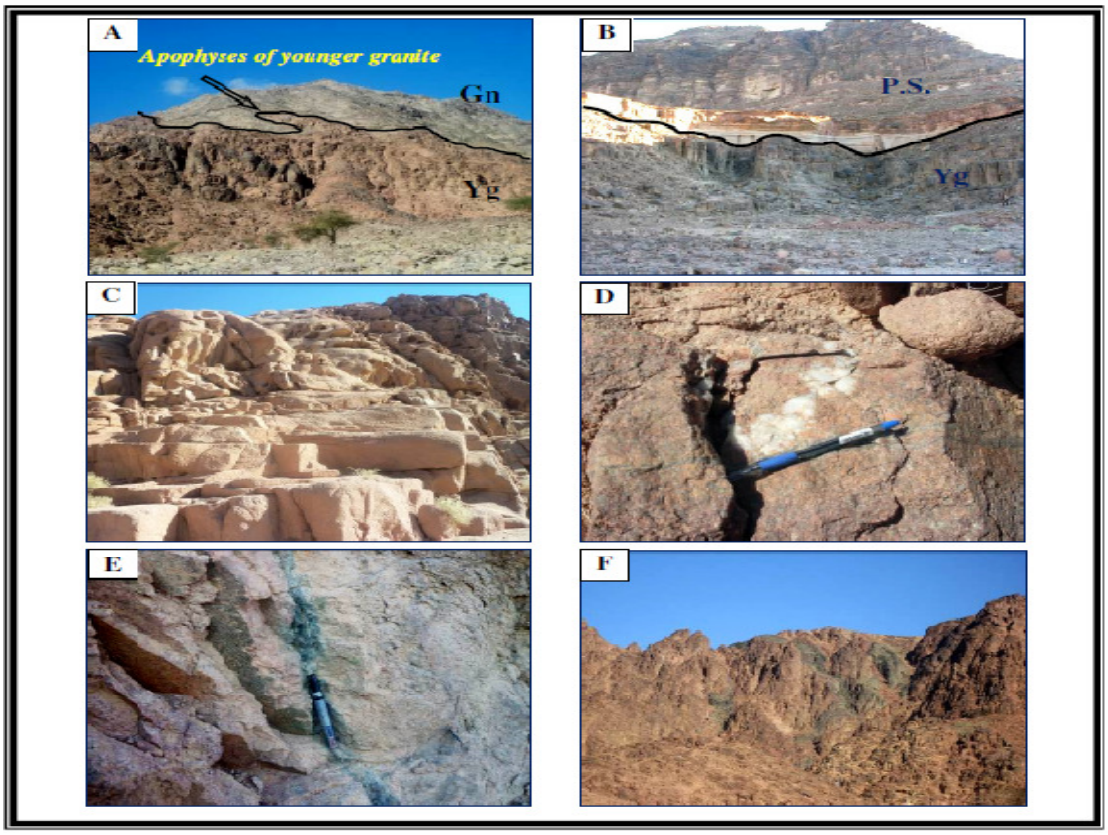

Figure 3: Photographs showing field description of younger granites and post granitic dykes.

A. Sharp intrusive contact between gneisses (Gn) and younger granites (Yg). Apophyses of younger granites intrude gneisses rocks, Wadi Seih area.
B. The younger granites (Yg) are capped by Paleozoic sedimentary succession (P.S.), Wadi El Sahu area.
C. Jointing and cavernous phenomena appear on the weathered surfaces of younger granites, Wadi El Sahu area.
D. Pocket of pegmatite within younger granites, Wadi El Sahu area.
E. Fluorite-bearing quartz vein cutting through the younger granite of Gabal Adediya, Wadi El Sahu area.
F. Dyke swarms cutting through younger granites, Wadi El Tiyour area.

Petrographic Description

The microscopic examinations are carried out on the studied basement rock units to determine their mineralogical composition and textural relationships. Twenty one samples were selected (9 gneisses, 12 younger granites), prepared as thin sections and studied by transmitted polarized light microscope.

Gneisses

Gneisses are represented by paragneiss as garnet-biotite gneiss and orthogneiss as biotite-hornblende gneiss. The paragneiss consists of plagioclase and quartz together with biotite and muscovite. Garnet, chlorite and epidote occur as secondary minerals, while apatite, iron oxides and zircon as accessory minerals. Plagioclase is the main feldspar occurring as highly deformed crystals forming augen-like texture where the crystals are stretched and characterized by wedged ends (Fig. 4A). Some crystals of plagioclase are highly saussuritized or altered to epidote and carbonate minerals (Fig.4B).Quartz is elongated forming ribbon texture and shows microfolding (Fig.4C) due to deformation effects. It is mostly brecciated and presents as angular strained grains showing undulose extinction (Fig.4B).

Biotite is characterized by strong pleochroism and ranges in color from pale brown to dark brown. In most cases, biotite is stretched, producing kinked bands and gneissose texture which is mainly due to deformation effects. In some cases, biotite is altered to chlorite liberating iron oxides along its cleavage planes (Fig.4C). Muscovite presents as an alteration product of potash feldspars "secondary muscovite" (Fig. 4D). Secondary epidote is recorded associating biotite (Fig.4E), while garnet occurs as large cracked xenoblastic porphyroblasts, mostly associated with biotite suggesting that garnet originated by metasomatism of biotite to chlorite and then to garnet(Fig. 4F).Accessory minerals are generally represented by apatite which occurs as broad crystals wrapped by flakes of biotite (Fig. 4G). Zircon is also present as euhedral crystals showing pleochroic haloes included in biotite (Fig.4H).

Orthogneiss consists of plagioclases and quartz as the main felsic minerals associated with hornblende and biotite as the main mafic minerals. Apatite, zircon, allanite and xenotime are the main accessory minerals.

Plagioclase is the main feldspar appearing as hypidioblastic and xenoblastic crystals with cloudy appearance. It is characterized by albite and albite/percline twinning (Fig. 5A).They are highly deformed as indicated by the presence of augen-like texture where the crystals are stretched and characterized by pointed ends (Fig. 5B). Some crystals of plagioclase are affected by tectonism exhibiting parting and dislocation; it is occasionally altered to saussurite and epidote minerals. Quartz exhibits its characteristic wavy extinction. In some cases, quartz is strained, elongated and characterized by undulose extinction corroding the pre-existed plagioclase and biotite.

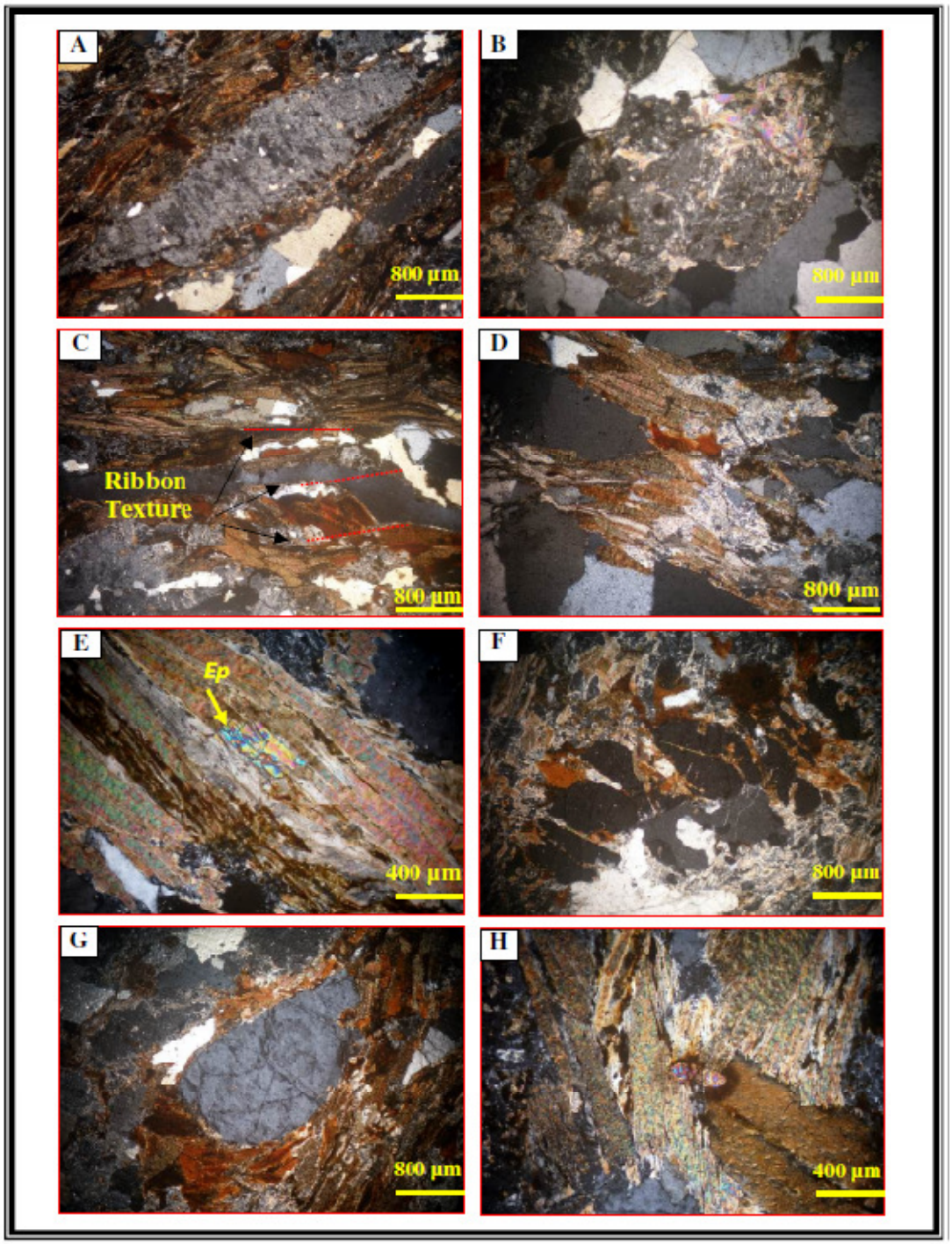

Figure 4: Photomicrographs for the studied paragneiss (garnet-biotite gneiss).

A. Highly deformed crystal of zoned plagioclase with wedged ends surrounded by biotite and quartz, CN.
B. Plagioclase altered to saussurite and carbonate minerals, CN.
C. Foliated flakes of biotite forming gneissose texture associated with elongated and strained crystals of quartz exhibit ribbon texture, CN.
D. Biotite flakes partially transformed to chlorite, CN.
E. Secondary epidote (*ep*) associating biotite, CN.
F. Secondary garnet is highly deformed and fractured, CN.
G. Broad crystal of apatite wrapped by biotite, CN.
H. Fractured crystal of zircon surrounded by plecchroic haloes included in biotite, CN.

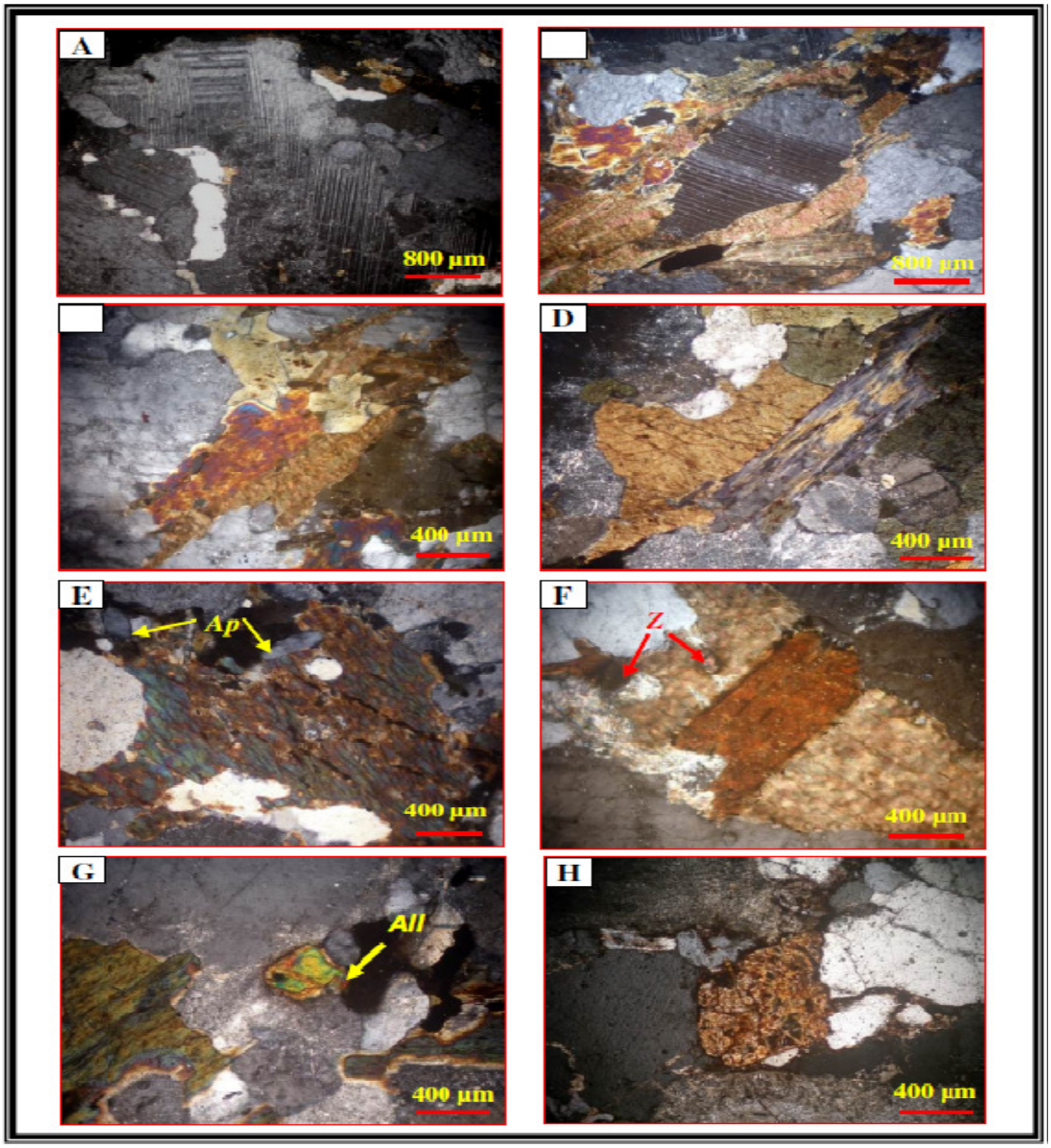

Figure 5: Photomicrographs for the studied orthogneiss (biotite-hornblende gneiss).

A. Subhedral crystals of plagioclase showing percline and albite twinning, CN.
B. Augen-like texture showing stretched crystal of plagioclase with pointed ends, CN.
C. Hornblende ispartially altered to biotite and actinolite, CN.
D. Hornblende partially altered to chlorite of penninite type, CN.
E. Euhedral crystals of apatite (*Ap*) included in hornblende, CN.
F. Euhedral crystals of zircon (*Zr*) surrounded by pleochroic haloes included in biotite, CN.
G. Well-formed crystal of allanite (*All*) imbedded in altered plagioclase, CN.
H. Intensively metamictized crystal of xenotime showing radial fractures associating quartz and plagioclase, CN.

Hornblende is characterized by strong pleochroism ranging in color from pale brown to dark green. It occurs as hypidioblastic and xenoblastic crystals with deep green color and exhibits its characteristic two sets of cleavage. Sometimes, hornblende is intensively altered where the alteration process initiates at the core of the crystals and gradually increases outward. It is also gradually altered to biotite, actinolite (Fig. 5C) and chlorite (Fig. 5D) suggesting low grade retrograde metamorphism. Biotite is characterized by strong pleochroism ranging in color from pale brown to dark brown. Sometimes, it is found as an alteration product of hornblende showing distinctive cleavage (Fig. 5C). Sometimes, biotite is stretched parallel to its longest axis alternating with the quartzo-feldspathic components producing the gneissose texture. It is also altered to chlorite referring to low to moderate temperatures (Shelley 1993). Chlorite is characterized by low to moderate pleochroism and ranging in color from pale green to dark green. In some cases, chlorite shows penninite type with blue interference color (Fig. 5D).

Accessory minerals are generally represented by apatite which occurs as euhedral crystals embedded in hornblende (Fig. 5E). Zircon is also present as euhedral crystals embedded in biotite and surrounded by pleochroic haloes (Fig. 5F). These haloes result from the radiation effects of the radio elements included in the internal structure of zircon. Allanite is found as euhedral crystals included in plagioclase and showing its characteristic interference color (second order), (Fig. 5G). A strongly metamictized crystal characterized by radial fracture is recorded associating quartz and plagioclase; may be xenotime (Fig. 5H).

Younger Granites

The modal analyses of Wadi El Sahu younger granites (Table-1)are plotted on Streckeisen (1976) diagram (Fig. 6). It is clear that, the studied younger granites fall in monzogranite and syenogranite fields.

Table 1: Modal analyses for Wadi El Sahu Younger granites

Rock Type	Sample No.	Quartz	Plag.	Potash Feld.	Mafics	Opaque & Acc.
Monzo granite	S8	26.7	39.3	32.5	1.5	0.0
	S16	29.5	37.4	27.4	3.2	2.5
	S25	32.5	35.3	29.2	1.8	1.2
	UH3	30.7	27.8	37.9	2.8	0.8
	FS	24.7	40.6	30.8	2.2	1.7
	T4	22.3	38.6	35.3	2.6	1.2
	SH2	27.5	36.8	32.3	1.9	1.5
	Av	**27.7**	**36.5**	**32.2**	**2.30**	**1.3**
Syeno granite	S1	30.5	10.3	56	1.8	1.4
	S4	29.4	11.4	58.3	0.6	0.3
	AS	25.3	12.1	57.9	3.5	1.2
	S7	32.9	8.2	54.6	1.5	2.8
	S12	22.7	8.0	63.3	3.8	2.2
	Av	**28.16**	**10**	**58.02**	**2.24**	**1.58**

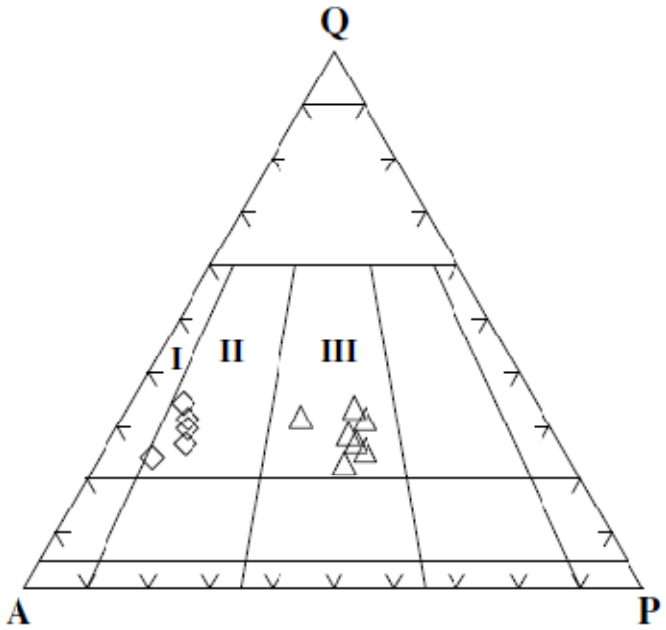

Figure 6: Classification of the younger granites of Wadi El Sahu, Streckeisen, (1976).
I= Alkali feldspar granite, iI= syenogranite and III= monzogranite

Monzogranite

Microscopically, it consists of plagioclase (36.5%), K-feldspar (32.2%) and quartz (27.7%) together with biotite and muscovite. It is medium-grained and characterized by grayish pink color and equigranular texture.

Plagioclase (An_{16}) occurs as subhedral to euhedral crystals of oligoclase showing cloudy appearance with albite and percline twinning(Fig. 7A). It occasionally occurs as fine crystals of albite poiklitically included in K-feldspars (Fig.7B). Some crystals show myrmekitic texture where quartz occurs as vermicules (Fig.7C). K-feldspar occurs as subhedral crystals of perthite and antiperthite. Perthite is mainly represented by string and patchy types (Fig.7D). Antiperthite presents as flame type enclosing finer crystals within plagioclase (Fig.7E). Quartz occurs as anhedral crystals associating the main constituents (plagioclase and K-feldspar) or as skeletal crystals graphically inter grown with K-feldspar forming micrographic texture (Fig.7F).

Biotite is the least common constituent (2.3%) generally characterized by strong pleochrism and ranging in color from pale brown to dark brown. Sometimes, it is partially altered to chlorite (Fig.8A). Muscovite is characterized by high interference color (Fig.8B) and sometimes presents as alteration product of plagioclase and biotite.

Accessory minerals are mainly zircon which occurs as euhedral crystals with zonation and partially metamictized included in perthite (Fig.8C). Fluorite is found as large crystals of colorless and violet colors. It exhibits subhedral to euhedral interstitial crystals (Fig.8D). Allanite occurs as euhedral crystals of reddish brown color associating biotite and plagioclase (Fig.8E). Xenotime is found as fractured crystal included in biotite (Fig.8F).

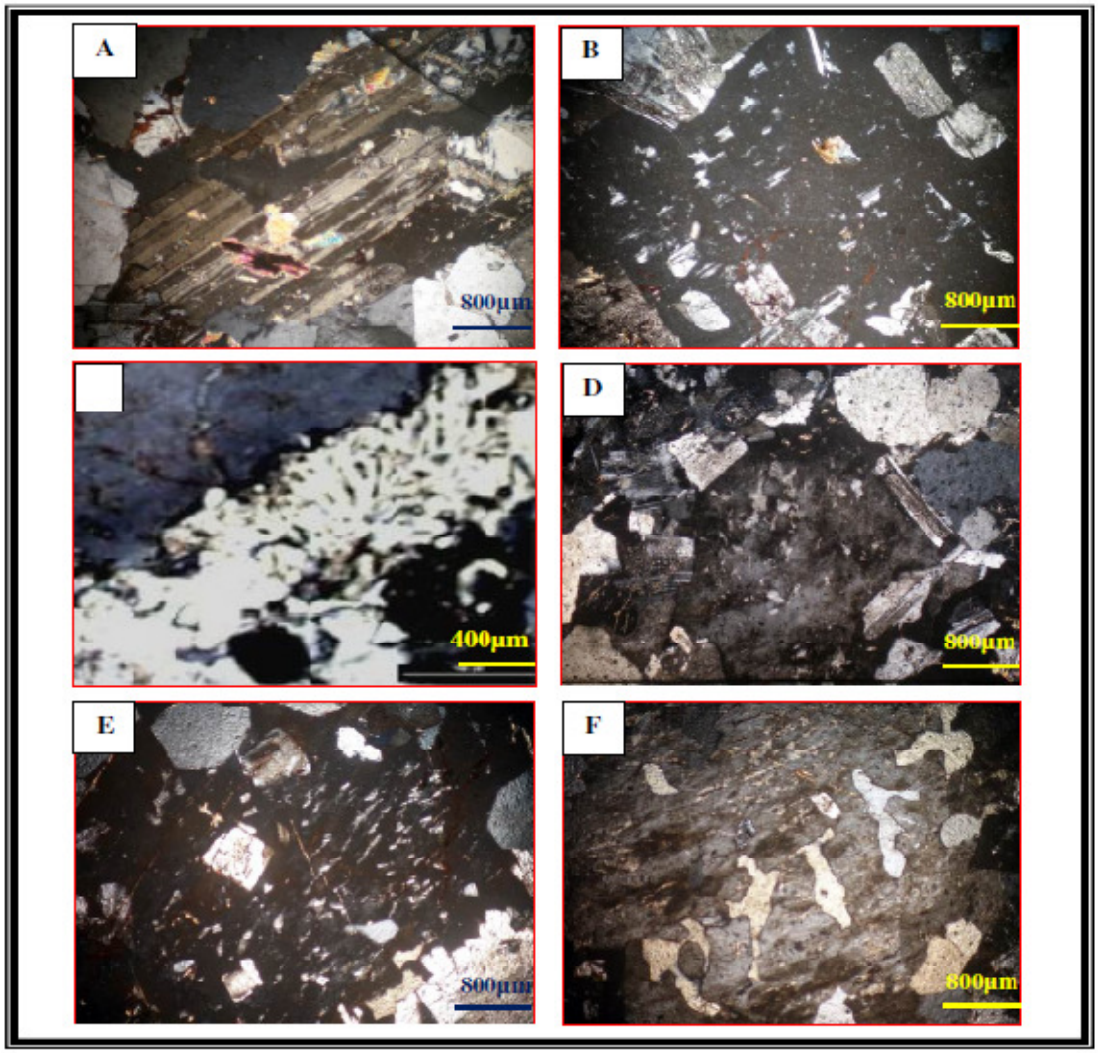

Figure 7: Photomicrographs for the studied monzogranite.

A. Subhedral crystal of plagioclase with lamellar twinning partially altered to epidote, CN.
B. Fine crystals of albite poiklitically included in K-feldspars, CN.
C. Myrmekitic texture developed along the plagioclase-potash feldspar boundary, CN.
D. Anhedral crystal of patchy perthite associating plagioclase and quartz, CN.
E. Anhedral crystal of flame antiperthite includes albite crystals and associates quartz, CN.
F. Quartz is micrographically intergrown with perthite, CN.

Syenogranite

Microscopically, it consists of K-feldspars (58.02%), plagioclase (10.0%) and quartz (28.16%) together with biotite and muscovite. It ranges in color from buff to pink with medium-grain size.

K-feldspars are mostly represented by orthoclase, orthoclase-perthite and microcline. Orthoclase shows its characteristic simple twinning of Carlsbad type (Fig.9A). Perthite is widely distributed as well developed crystals of orthoclase-perthite (Fig.9B). Microcline is represented by little subhedral crystals with a characteristic cross-hatching twinning (Fig.9C). Alteration of K-feldspars to sericite is common. Plagioclase is more sodic (An_{8-12}), appears as subhedral to euhedral crystals of albite and oligoclase and shows cloudy appearance with albite and percline twinning. Plagioclase is partly altered to sericite (Fig.9D). Quartz presents as primary crystals associating the other constituents or as fine crystals resulting from reworking of the primary ones or due to silisification processes (Fig.9E).

Biotite is generally characterized by strong pleochrism and ranging in color from pale brown to dark brown. Sometimes, it is partially altered to chlorite especially along its cleavage planes in association with iron oxide (Fig.9F). Muscovite presents as flakes with fan-shaped and characterized by high interference color (Fig.9G) and sometimes presents as secondary muscovite as an alteration product of K-feldspars.

Zircon is the only accessory mineral present as euhedral crystals showing 2nd order interference color and surrounded by pleochroic haloes (Fig. 9H).

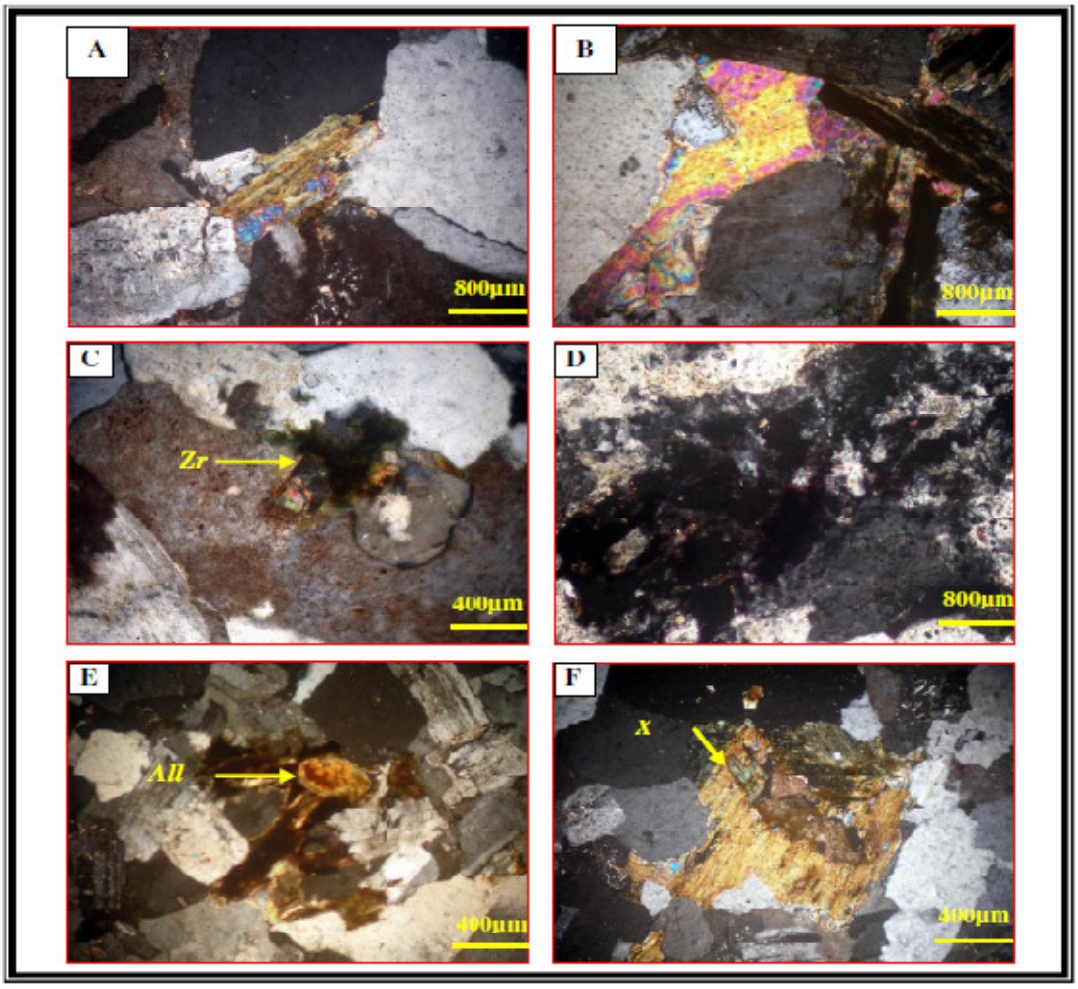

Figure 8: Photomicrographs for the studied monzogranite

A. Biotite partially altered to chlorite and muscovite associating plagioclase and quartz, CN.
B. A flake of muscovite associating biotite and plagioclase, CN.
C. Euhedral crystal of zircon(*Zr*) shows color zonation and partially metamictized included in perthite, CN.
D. Euhedral to subhedral crystals of fluorite with violet color, CN.
E. Euhedral crystal of allanite (*All*) associating biotite and plagioclase, CN.
F. Fractured crystal of xenotime (*X*) included in biotite, CN.

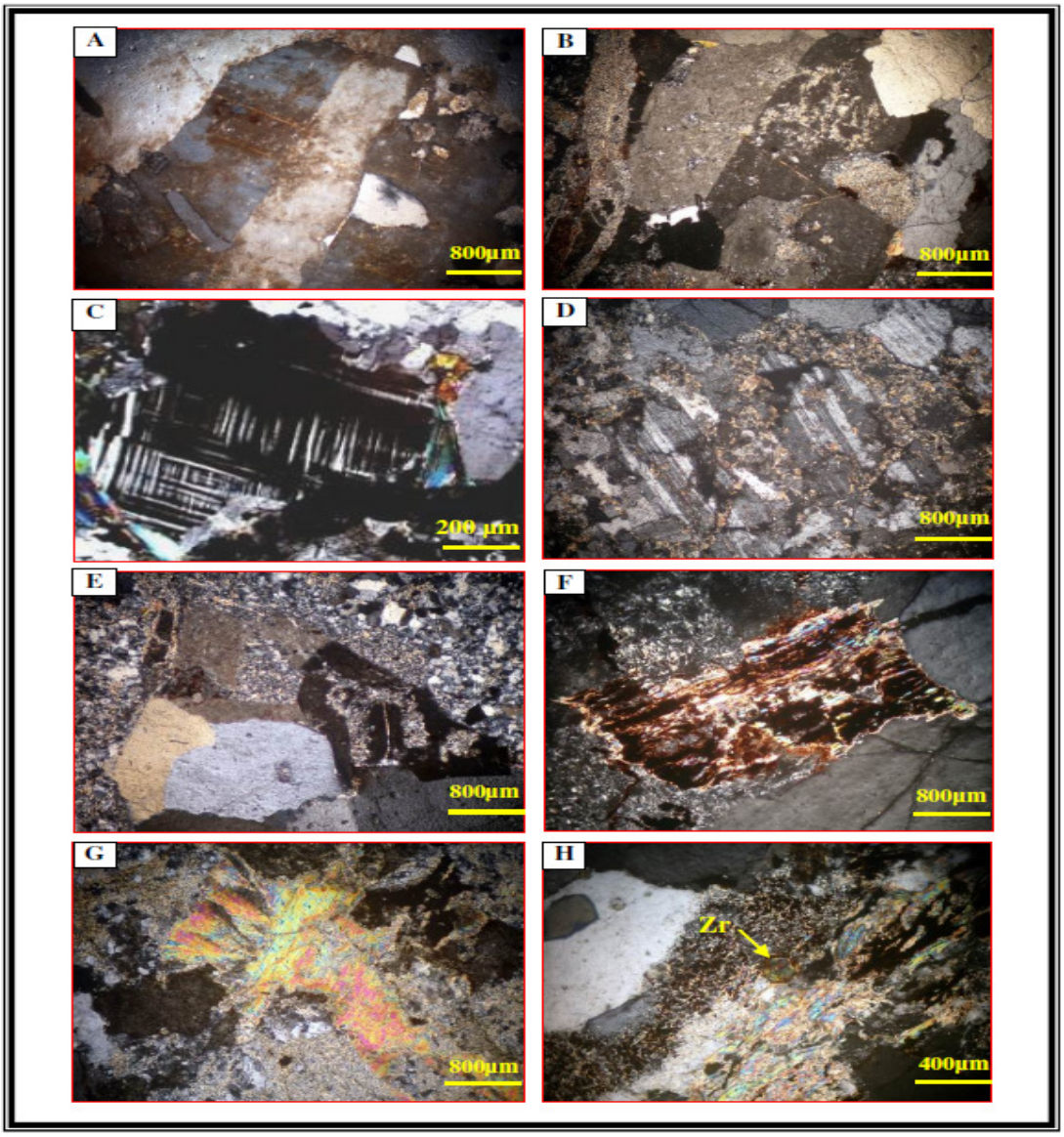

Figure 9: Photomicrographs for the studied syenogranite.

A. Euhedral crystal of orthoclase showing simple twinning stained by iron oxide, CN.
B. Anhedral crystal of orthoclase- perthite corroded by quartz and partially sericitized, CN.
C. Subhedral crystal of microcline with a characteristic cross-hatching twinning, CN.
D. Plagioclase partially altered to muscovite and sericite, CN.
E. Primary quartz associating secondary quartz as reworked silica, CN.
F. Flake of biotite intensively altered to chlorite and iron oxide, CN.
G. Flake of muscovite with fan-shaped, CN.
H. Euhedral crystal of zircon (*Zr*) surrounded by pleochroic haloes included in secondary muscovite, CN.

Geochemistry

The chemical analyses of major oxides and trace elements of 21 representative samples from the gneisses (9 samples) and the younger granites (12 samples) were carried out in the Laboratories of Nuclear Materials Authority. The major oxides were determined by using wet chemical analytical technique (Shapiro and Brannock, 1962) and the trace elements were determined by using X-ray fluorescence technique by Philips X-ray spectrometer (X-Unique II) with automatic sample changer PW-1510.

Gneisses

The studied gneisses were classified petrographically as paragneiss and orthogneiss; the orthogneiss is characterized by higher SiO_2 (av. = 64.8 %), CaO (av. =3.74%) and Na_2O (av. =3.85%) contents rather than the paragneiss; while the other oxides are lower (Table-2).

Table 2: Chemical analyses of the studies gneisses comprising the major oxides (%) and trace elements (ppm)

Rock	Paragneiss				Orthogneiss						
S.No.	T2	T3	T5	Av.	Se3	Se4	Se5	Se8	Se9	Se10	Av.
Major oxides (%)											
SiO_2	58.14	56.8	61.1	58.68	63.8	64.2	65.5	65.3	67.1	62.92	64.8
Al_2O_3	16.93	17.62	16.17	16.91	15.5	15.3	14.8	14.9	14.5	15.3	15.05
TiO_2	1.12	1.15	1.05	1.11	0.5	0.48	0.45	0.52	0.42	0.62	0.5
$Fe_2O_3^t$	7.5	8.7	6.5	7.57	6.3	5.7	6.3	6.9	5.7	2.5	5.57
MgO	3.56	3.14	3.33	3.34	1.5	1.9	1.55	1.33	1.2	3.96	1.91
CaO	3.44	2.9	3.12	3.15	4.9	4.3	3.7	3.2	2.6	3.73	3.74
K_2O	2.05	1.85	2.24	2.05	1.4	1.8	1.7	2.1	2.2	1.65	1.81
Na_2O	3.88	3.28	3.6	3.59	3.8	3.7	3.3	3.5	3.2	5.6	3.85
P_2O_5	0.32	0.42	0.28	0.34	0.10	0.17	0.22	0.14	0.15	0.56	0.22
L.O.I	1.9	2.49	2.1	2.16	2.5	2.4	2.8	2.2	2.6	2.8	2.55
Total	99.84	98.35	99.49	98.89	100.3	99.95	100.32	100.09	99.67	99.64	99.99
Geochemical parameters											
MgO/CaO	0.29	0.37	0.27	0.31	0.20	0.35	0.49	0.27	0.36	0.90	0.43
$P2O_5/TiO_2$	1.03	1.08	1.07	1.06	0.31	0.44	0.42	0.42	0.46	1.06	0.52
Trace elements (ppm)											
Cr	82	77	67	75.33	65	42	41	69	75	37	54.83
Ni	37	34	29	33.33	22	18	19	20	29	15	20.5
Cu	2266	45	51	787.33	42	49	61	51	41	61	50.83
Zn	89	83	91	87.67	55	81	67	71	75	79	71.33
Zr	85	87	72	81.33	94	92	101	96	99	88	95
Rb	79	72	81	77.33	35	48	53	46	66	70	53
Y	7	9	11	9	6	9	11	9	7	5	7.83
Ba	2428	1820	2110	2119	1984	1712	1842	2187	2417	1553	1949
Pb	9	12	11	10.67	14	28	27	26	22	34	25.17
Sr	128	111	117	118.67	155	147	139	141	150	153	147.5
Ga	9	8	8	8.33	14	14	13	16	12	17	14.33
V	108	98	112	106	93	96	88	91	101	80	91.5
Nb	5	6	5	5.33	5	7	6	8	5	5	6

Plotting of the studied gneisses on the discrimination diagram of Tarney (1977) using SiO_2 versus TiO_2 localized the three samples of paragneiss in the field of sedimentary origin while the six samples of the orthogneiss fall in the field of igneous origin (Fig.10). The same origin was confirmed by using the ratios MgO/CaO versus P_2O_5/TiO_2 on the discrimination diagram of Werner (1987), (Fig. 11).

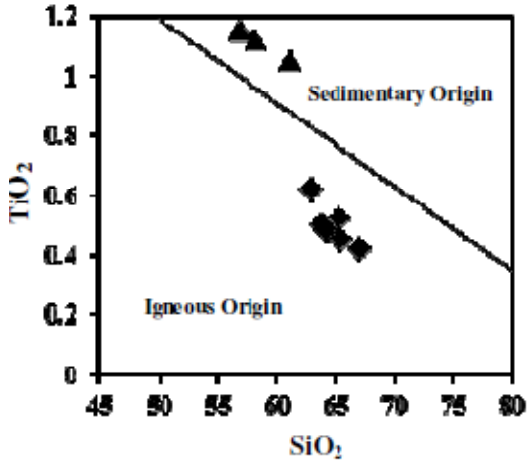

Figure 10: SiO_2 versus TiO_2 discrimination diagram for the studied gneisses, Tarney (1977).
Paragneiss = ▲ Orthogneiss = ♦

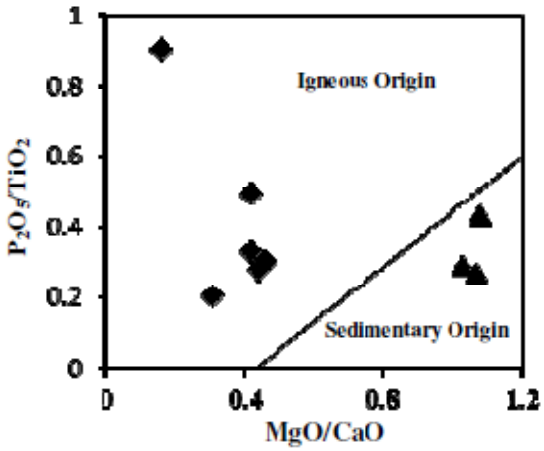

Figure 11: MgO/CaO versus P_2O_5/TiO_2 discrimination diagram for the studied gneisses, Werner (1987). *Symbols as in fig. 10.*

The plotting of SiO_2 versus K_2O for the studied orthogneiss shows positive correlation (Fig. 12), while plotting of SiO_2 versus CaO shows negative correlation (Fig. 13), so the studied orthogneiss has an igneous origin according to Tarney (1977),who stated that many igneous rocks have well-defined positive correlation between SiO_2 and K_2O and well-marked negative correlation between SiO_2 and CaO.

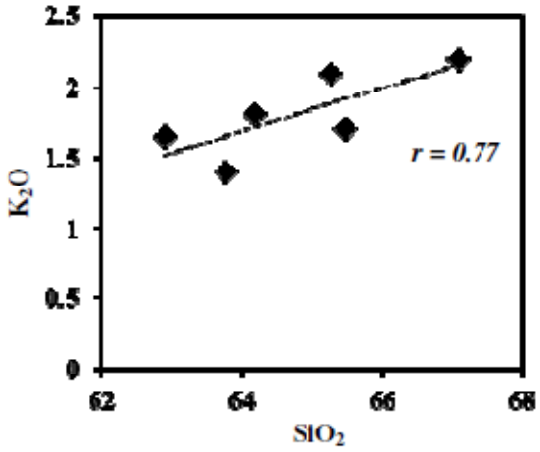

Figure 12: Binary relation between SiO_2 versus K_2O in the studied orthogneiss. *Symbols as in fig. 10.*

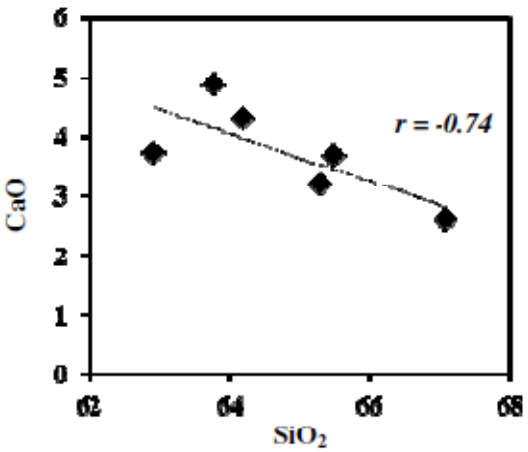

Figure 13: Binary relation between SiO_2 versus CaO in the studied orthogneiss. *Symbols as in fig. 10.*

The studied gneisses are characterized by high Ba content up to 2428 ppm referring to substitution of Ba to Ca content in calcic minerals (hornblende and plagioclase). The paragneiss is distinguished by high Cu content (anomalous) up to 2266 ppm (Table-2). The trace element concentrations are normalized by continental crust values, Weaver and Tarney (1984) for the two types of gneiss indicating similarity of the two spiders except for Pb and Cu which are higher in the paragneiss rather than the orthogneiss. The two spiders show enrichment of Ba, Rb and Pb while the Cu is highly enriched in the paragneiss only. The other trace elements are depleted in both of their gneisses (Fig. 14).

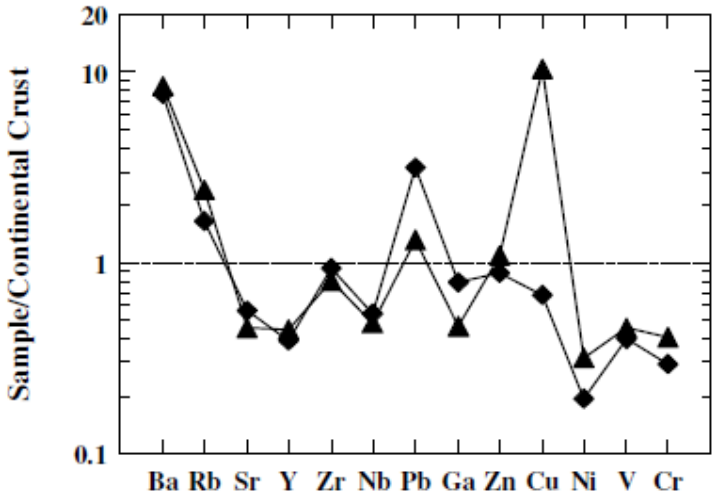

Figure 14: Trace elements of the studied gneisses normalized by Continental Crust values, Weaver and Tarney (1984). Symbols as in fig. 10.

Younger Granites

The studied younger granites were classified petrographically into monzogranite and syenogranite. The norm values of the two types are plotted on the classification diagram of Strekeisen (1976) indicating that the two types are falling in the monzogranite and syenogranite fields (Fig. 15).

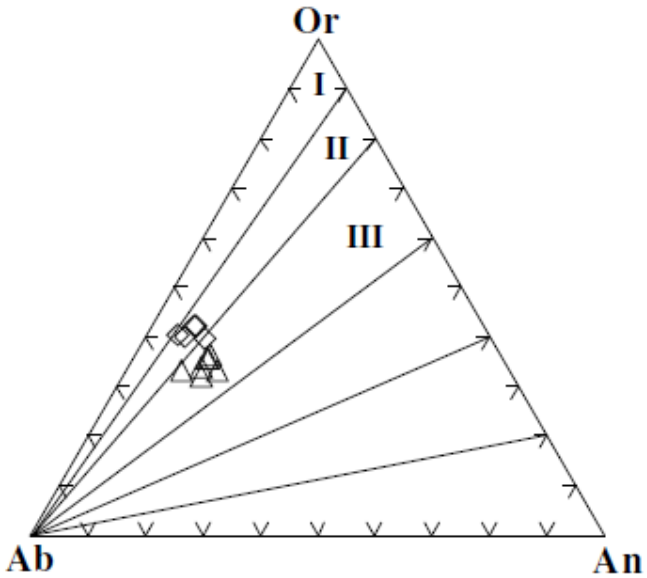

Figure 15: Classification of the studied younger granites by using norm values, Strekeisen (1976).

I= Alkali feldspar granite, II= syenogranite(◊) and III=monzogranite (Δ)

Chemical characteristics

The syenogranite is characterized by high SiO_2 (av. = 74.64%), K_2O (av. = 4.15%) and Na_2O (av. = 3.66%); the other oxides are relatively lower than the corresponding values in the monzogranite (Table-3).

Table 3: Chemical analyses of the studied younger granites comprising the major oxides (%), trace elements (ppm), norm values and some geochemical parameters

Rock	Monzogranite								Syenogranite					
S.No.	S8	S16	S25	T4	FS	UH3	SH2	Av.	S1	S4	S7	S12	AS	Av.
Major Oxides (%)														
SiO_2	71.5	72.05	72.1	72.61	71.75	71.85	71.8	71.95	75.0	74.3	74.5	74.6	74.82	74.64
Al_2O_3	13.95	14.6	14.6	13.85	14.57	14.54	14.81	14.42	13.2	12.5	12.9	13.2	12.62	12.88
TiO_2	0.01	0.01	0.01	0.06	0.13	0.11	0.13	0.07	0.01	0.01	0.01	0.01	0.12	0.03
$Fe_2O_3^t$	2.8	2.3	2.1	1.32	1.5	2.33	1.83	2.03	1.7	1.9	1.7	1.5	1.62	1.68
MgO	0.9	0.8	1	1.16	1.48	1.3	1.1	1.1	0.6	0.7	0.8	0.8	0.6	0.7
CaO	1.5	1.8	1.4	1.71	1.83	1.62	1.58	1.63	0.9	1	1.3	0.9	1.18	1.06
K_2O	3.31	3.1	3.4	3.8	3.25	3.68	2.81	3.34	4.1	4.3	4	4.1	4.24	4.15
Na_2O	3.7	3.3	3.3	3.8	3.92	3.7	3.4	3.59	3.4	4	3.5	3.5	3.9	3.66
P_2O_5	0.01	0.01	0.01	0.06	0.06	0.01	0.08	0.03	0.04	0.01	0.01	0.01	0.01	0.02
L.O.I	1.6	1.7	1.75	1.5	1.59	1.52	1.72	1.63	0.55	0.5	0.85	0.9	1.05	0.77
Total	99.28	99.67	99.67	99.87	100.08	100.66	99.26	99.78	99.5	99.22	99.57	99.52	100.16	99.59
Norm Values														
Q	33.53	36.76	36.2	31.25	32.23	31.11	37.38	34.07	37.46	32.48	35.65	36.27	33.44	35.06
Or	20.01	18.71	20.54	22.85	19.41	21.97	17.04	20.08	24.53	25.76	23.97	24.59	25.3	24.83
Ab	31.96	28.45	28.48	32.65	33.45	31.56	29.46	30.86	29.07	34.24	29.96	29.29	33.26	31.16
An	7.55	9.06	7.04	8.27	5.62	8.06	7.56	7.59	4.28	3.46	6.48	4.47	4.41	4.62
Geochemical parameters														
D.I.	85.54	84.42	85.18	86.91	84.22	84.52	82.12	84.70	91.07	91.87	89.95	91.20	91.96	91.21
A.R.	0.45	0.4	0.4	0.48	0.42	0.44	0.36	0.42	0.54	0.63	0.58	0.54	0.64	0.59
Trace Elements (ppm)														
Cr	25	27	31	21	25	28	25	26	40	21	22	25	40	29.6
Ni	11	9	8	9	10	9	7	9	10	7	8	12	13	10
Cu	10	12	11	13	11	10	11	11.14	10	12	11	17	11	12.2
Zn	36	31	43	36	32	37	33	35.43	29	35	27	66	48	41
Zr	147	157	162	174	200	194	150	169.14	167	165	184	170	136	164.4
Rb	165	194	120	156	159	161	193	164	445	304	317	266	284	323
Y	26	32	31	36	28	25	26	29	82	79	88	85	66	80
Ba	279	225	368	159	195	312	222	251	222	144	222	321	279	238
Pb	37	33	18	32	22	13	39	27.71	19	18	11	28	11	17.4
Sr	30	30	36	36	42	48	24	35	30	30	42	36	24	32
Ga	21	21	15	20	13	12	21	17.57	13	14	10	17	11	13
V	6	3	9	6	6	9	3	6	6	3	6	9	15	8
Nb	10	13	13	15	20	19	11	14.4	28	28	31	30	22	27.8

D.I. = Differentiation Index A.R. = Alkalinity Ratio

The two types of younger granites are characterized by high differentiation indexes where the syenogranite is higher (from 89.95 to 91.96) than the monzogranite (from 82.12 to 86.91).

The plotting of studied younger granites on the discrimination diagram of Shand (1951) showing that they lie in the field of peraluminous except for two samples of syenogranite which are falling in the field of metaluminous close to the separating line indicating that the syenogranite is lower than the monzorgranite in alumina content (Fig. 16).

Alkalinity ratio of the studied younger granites is represented graphically versus silica content on Wright diagram (1969). It is clear that the two types are moderately alkaline where monzogranite samples are located on the lower limit of the moderate alkaline field, while the syenogranite samples are located on the upper limit of the moderate alkaline field (Fig. 17).

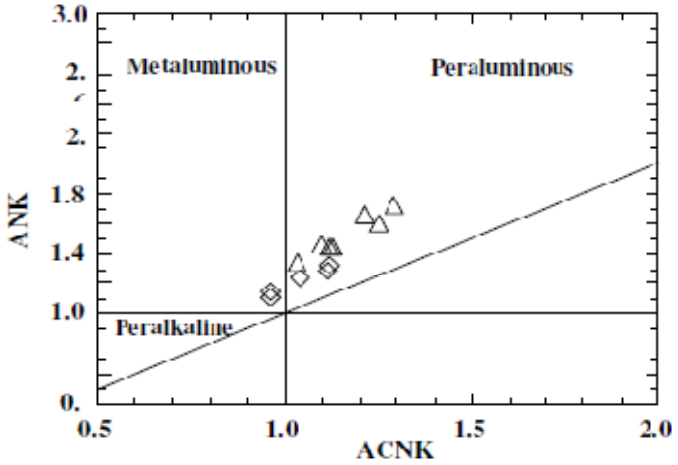

Figure 16: Shand index diagram for the younger granites, Shand (1951).
ANK= Al_2O_3/ (Na_2O+K_2O) & ACNK= Al_2O_3/ (CaO+Na_2O+K_2O)
Symbols as in fig. 15.

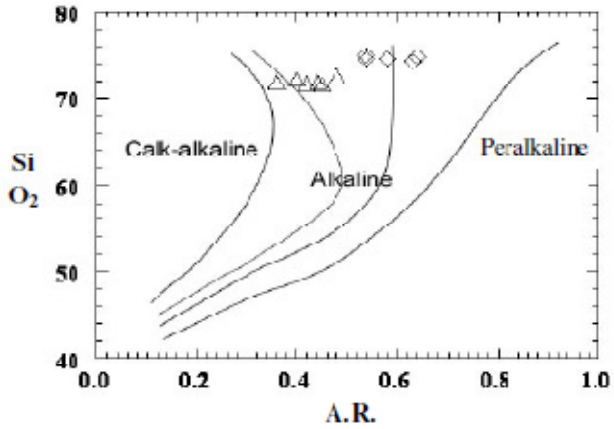

Figure 17: SiO_2 vs. alkalinity ratio (A.R.) for the studied younger granites,Wright (1969). *Symbols as in fig. 15.*

The trace element concentrations are normalized by continental crust values of Weaver and Tarney (1984)for the two types of younger granite indicating similarity of the two spiders. The two spiders show enrichment of Rb, Y, Zr, Nb and Pb while the other trace elements are depleted in both of their younger granites (Fig. 18).

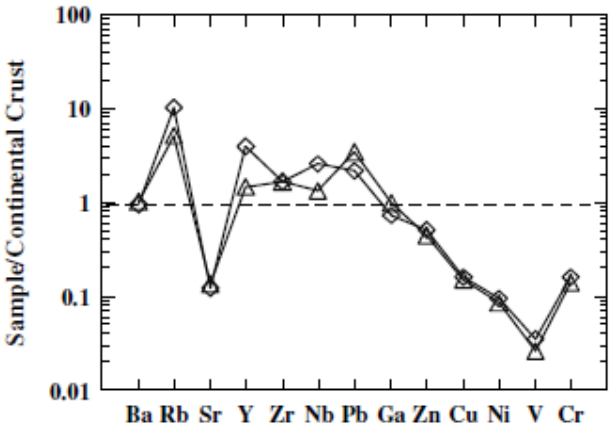

Figure 18: Trace elements of the studied younger granites normalized by continental crust values, Weaver and Tarney (1984). *Symbols as in fig. 15.*

Petrogenetic Features

Petrogenetic features of the studied younger granites were deduced from different relations of the major oxides and others between the trace elements. The ternary relation between total alkalies, FeO^t and MgO, Petro et al. (1979) showing that, the studied younger granites follow the extensional trend (Fig. 19).

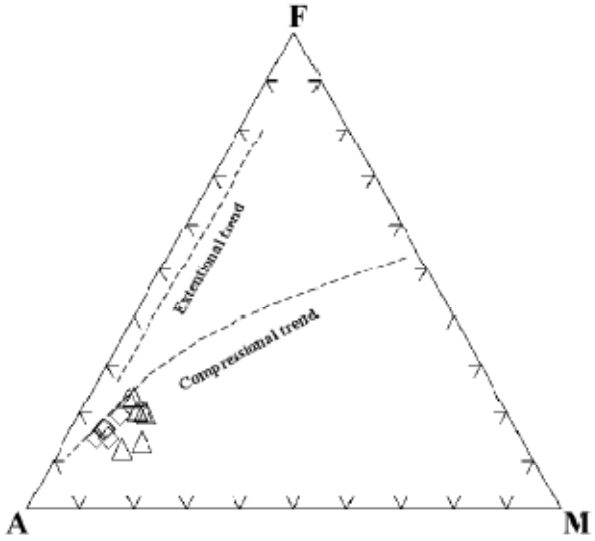

Figure 19: A.F.M ternary diagram for the studied younger granites, Petro et al., (1979). *Symbols as in fig. 15.*

The ternary relation Rb-Ba-Sr is used by El Bouseily and El Sokkary (1975) to classify the granites according to their degrees of differentiation. Plotting of the studied younger granites on this diagram clarified that the syenogranite samples fall in the field of highly differentiated granites (I),while the monzogranite samples fall in fields of highly differentiated (I) and normal granites (II), (Fig. 20).

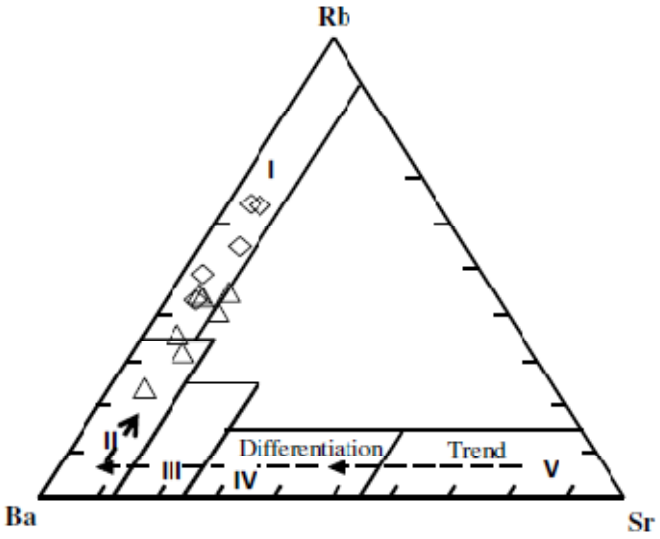

Figure 20: Rb-Ba-Sr ternary diagram for the studied younger granites, El Bouseily and El Sokkary (1975). *Symbols as in fig. 15.*
I =Strongly differentiated granite, II = normal granite, III=anomalous granite, IV=granodiorite & qz-diorite, V=Diorite.

Mineralogical composition of the granites calculated microscopically by modal analyses was used by Loiselle and Wones (1979) to conclude the magma type of the concerned granite. They modified the ternary relation of Strekeisen (1976) and subdivided the triangle to three fields (A-type, I-type and S-type granites). Plotting of quartz, alkali feldspar and plagioclase minerals of the studied younger granites on the diagram of Loiselle and Wones (op. cit.) located the syenogranite in the field of A-type, while the monzogranite is related to I-type, (Fig.21).

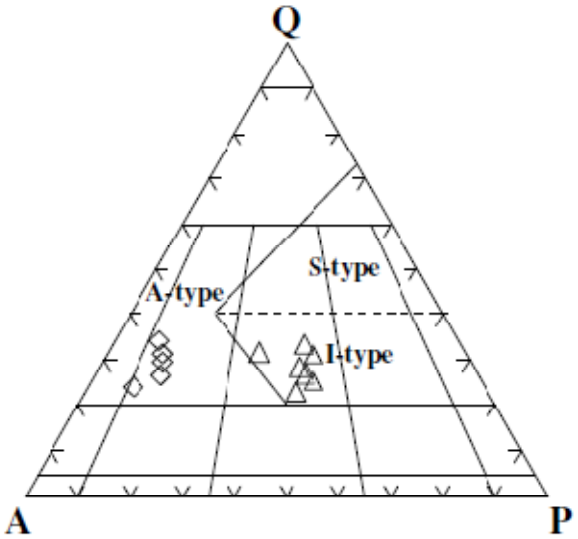

Figure 21: Q-A-P modal analyses diagram for the studied younger granites after Loiselle and Wones (1979). *Symbols as in Fig. 15.*

Tectonic Setting

Tectonic setting of the studied younger granites is deduced by using discrimination diagrams based upon major oxides and trace elements. Plotting of Al_2O_3 vs. SiO_2 for the analyzed samples of the two types on the discrimination diagram of Maniar and Piccoli, (1989) revealed that monzogranite and syenogranite belong to post-orogenic granite (POG), (Fig. 22).Trace elements are also used to conclude the tectonic setting by using the

discrimination diagram of Pearce et al., (1984). Plotting of Rb vs Y+Nb on this diagram located the monzogranite samples in the field of volcanic arc granite (VAG) while, the syenogranite samples fall in the field of within-plate granite (WPG), (Fig. 23).

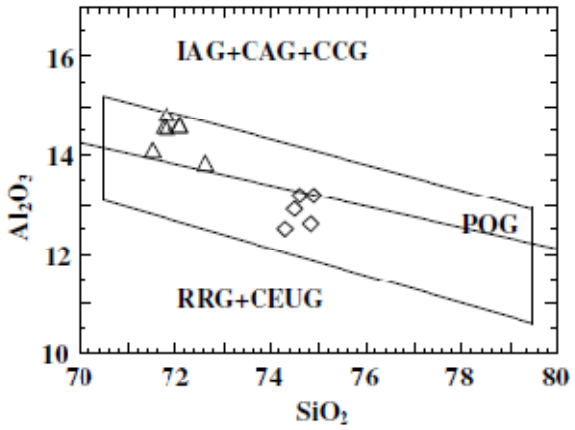

Figure 22: Discrimination diagram for tectonic setting of the studied younger granites, Maniar and Piccoli (1989). *Symbols as in fig. 15.*

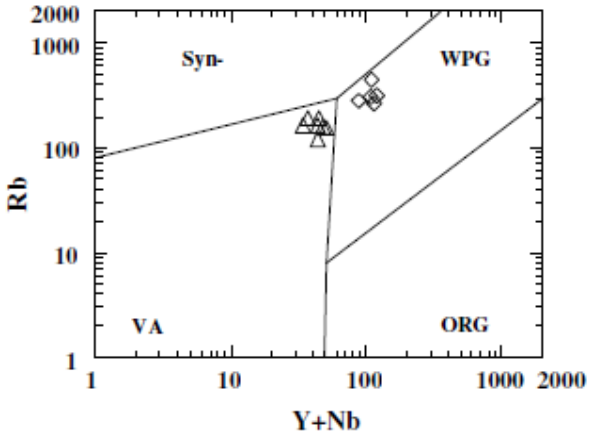

Figure 23: Discrimination diagram for tectonic setting of the studied younger granites, Pearce et al. (1984). *Symbols as in fig. 15*

Radioactivity

For a better determination of radioelement contents of the studied rock units, Bicron Scintillation Detector NaI (Tl) 76×76 mm is used to determine their uranium, thorium, radium and potassium contents. At first, the samples collected from different rock types were prepared for the radiometric measurements. In this stage, the rock samples were subjected to grinding in order to obtain crushed samples of about 0.5 mm grain size. Each sample was quartered using John's splitter to obtain a representative sample for the radiometric measurements. The obtained samples were packed in plastic containers, tightly sealed and stored for thirty days to be ready for the radiometric measurements. The analyzed rock units include; gneisses (ten samples) and younger granites (12 samples for monzogranite and 12 samples for syenogranites).

Distribution and Behavior of Radioelements in the Studied Rock Units

All the selected rock samples were analyzed radiometrically to determine their contents of eU, eTh, Ra (eU) (ppm) and K (%).The ratio eTh/eU was calculated as well as eU/ Ra (eU) ratio in order to test their radioactive equilibrium which would help to predict the U mobilization and the origin of mineralization, when present. The radiometric measurements of all rock units are given in (Table-4).Under magmatic conditions, thorium is generally three times more abundant than uranium; i.e. the Th/U ratio is generally about 3 (chondritic ratio). The eTh/eU ratios are controlled by redistribution of the uranium that in turn are controlled by the epigenetic

processes. The structural features play an important role in redistribution of uranium leading to depletion and/or enrichment.

Table 4: Radioactivity measurement ratios for the studied rock units

	Sample No.	eU (ppm)	eTh (ppm)	eU (Ra) (ppm)	K (%)	eTh/eU	eU/Ra
Gneisses	T2	4.00	9.00	5.00	5.39	2.25	0.80
	T3	5.00	8.00	5.00	2.29	1.60	1.00
	T5	3	6	3	2.29	2.00	1.00
	Se2	2.00	7.00	2.00	1.69	3.50	1.00
	Se3	1.50	7.00	1.00	1.49	4.67	1.50
	Se4	1.50	1.00	1.00	1.02	0.67	1.50
	Se5	1.50	3.00	1.00	1.18	2.00	1.50
	Se8	1.50	10.00	3.00	2.09	6.67	0.50
	Se9	2.00	8.00	4.00	2.27	4.00	0.50
	Se10	1.00	5.00	2.00	1.55	5.00	0.50
	Average	2.30	6.40	2.70	2.13	3.24	0.98
Monzogranite	4	35.00	39.00	25.00	2.04	1.11	1.40
	T1	11.00	34.00	13.00	3.70	3.09	0.85
	T4	20.00	39.00	13.00	3.83	1.95	1.54
	S8	18.00	34.00	13.00	3.73	1.89	1.38
	S10	14.00	40.00	11.00	3.85	2.86	1.27
	S16	10.00	37.00	7.00	3.85	3.70	1.43
	S24	11.00	34.00	8.00	3.84	3.09	1.38
	S25	14.00	26.00	8.00	3.94	1.86	1.75
	Sh1	10.00	34.00	7.00	3.17	3.40	1.43
	Sh2	16.00	36.00	6.00	3.83	2.25	2.67
	UH3	10.00	26.00	6.00	3.67	2.60	1.67
	FS	25.00	39.00	14.00	3.94	1.56	1.79
	Average	16.17	34.83	10.92	3.62	2.45	1.55
Syenogranite	1	16	16	9	2.3	1.00	1.78
	2	8	19	5	3.47	2.38	1.60
	5	11	12	5	1.8	1.09	2.20
	6	8	35	6	4.33	4.38	1.33
	8	16	32	8	4.39	2.00	2.00
	9	7	32	5	3.77	4.57	1.40
	S1	34.00	36.00	18.00	3.29	1.06	1.89
	S4	18.00	39.00	9.00	3.89	2.17	2.00
	S7	18.00	43.00	9.00	3.53	2.39	2.00
	S12	15.00	33.00	8.00	3.97	2.20	1.88
	S13	10.00	35.00	7.00	4.27	3.50	1.43
	AS	12.00	31.00	6.00	2.99	2.58	2.00
	Average	14.42	30.25	7.92	3.50	2.44	1.79

The studied gneisses are non-radioactive characterized by low uranium and thorium contents with an average eU=2.3 ppm and an average eTh=6.4 ppm (Table-4). The binary relation between eU and eTh shows positive relation with reasonable correlation coefficient (r=0.41) (Fig. 24) referring to absence of any metasomatic processes. The ratio eTh/eU (av.=3.24) approaching the chondritic value (3-3.5) Rogers and Adams (1969).

The studied younger granites are moderately radioactive where the monzogranite is relatively higher than the syenogranite. The former is characterized by an average eU=16.17ppm and an average eTh=34.43 ppm, while the syenogranite is characterized by an average eU=14.42ppm and an average eTh=30.25ppm.

For a better understanding of the behavior of uranium and thorium within the studied younger granites, their contents will be graphically represented. The binary relation between eU and eTh for the monzogranite revealed positive relation with reasonable correlation coefficient (r=0.49) referring to coexistence of the two radio elements in the source magma (Fig. 25). The same relation applied for the syenogranite clarified positive relation with weak correlation coefficient (r=0.31) referring to post-magmatic processes affecting on the redistribution of uranium(Fig. 26). The ratio eTh/eU for the monzogranite ranges between 1.11ppm and 3.7ppm, while in syenogranite it ranges between 1.0ppm and 4.57ppm; this variability in the ratio refers to migration of uranium (in and out).

The post granitic rocks (quartz-fluorite vein and basaltic dykes) represent abnormal anomalous sites (eU= 89ppm and eTh= 26ppm for the quartz-fluorite vein while the basaltic dykes contain eU= 98ppm and eTh = 10ppm).

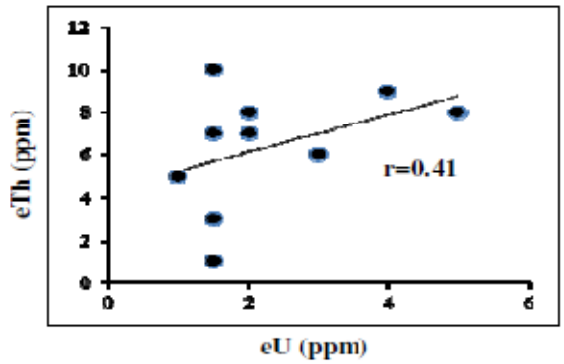

Figure 24: Binary relation between eU and eTh for the studied gneisses.

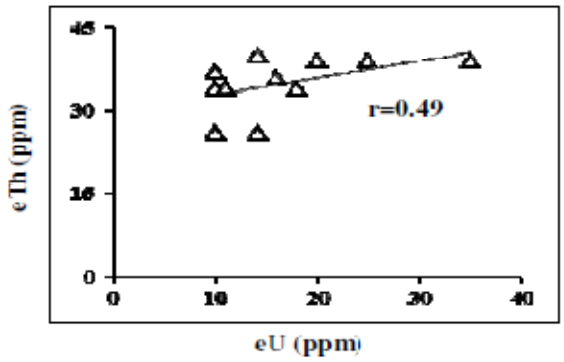

Figure 25: Binary relation between eU and eTh for the studied monzogranite.

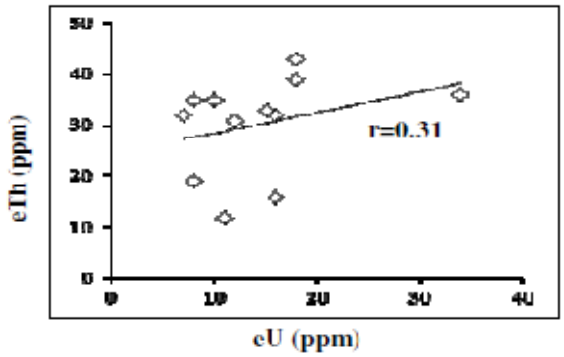

Figure 26: Binary relation between eU and eTh for the studied syenogranite.

Radioactive Equilibrium

The radioactive equilibrium/disequilibrium study is considered as an essential part in the radiometric investigation of U-ore deposits and U-bearing rocks; it can be used as a tool for U-exploration processes. In nature, the equilibrium state controlled by different geologic processes such as weathering, alteration, groundwater, meteoric water, circulating fluids through fractures and fault planes.

In the present study, the equilibrium/disequilibrium state was discussed through calculation of the equilibrium factor (P) which is defined as: P= eU/Ra (Hussein, 1978 and El Galy, 2003). The equilibrium state is reached, if the eU/Ra ratio is equal to unity. The obtained data in table (4) show that the studied gneisses approach the unity (P-factor=0.98) indicates nearly radioactive equilibrium. On the other hand, the studied younger granites are characterized by two states of disequilibrium (P-factors= 1.55 and 1.79for monzogranite and syenogranite respectively). The two values refer to enrichment of uranium contents rather than Ra.

CONCLUSIONS

- Wadi El Sahu environs is located in the southern part of Sinai Peninsula and covered with basement and sedimentary rocks. The basement rocks are represented by gneiss and younger granites, while the sedimentary succession is represented by clastic Paleozoic rocks.
- The field and petrographic investigations revealed that the studied gneissis classified into para and orthogneisses.The younger granites are classified microscopically intomonzogranite and syenogranite.
- Geochemically, the studied younger granites are peraluminous with alkaline affinity (moderately alkaline) originated in extensional regime. Monzogranite belongs to I-type granite formed in volcanic arc tectonic setting, while the syenogranite belongs to A-type formed in within-plate tectonic setting.
- The radioactivity of the studied gneisses is very low, while the younger granites are moderately radioactive. The monzogranite is relatively higher than the syenogranite. Both of them are characterized by variable eTh/eU ratios and disequilibrium state referring to mobility of uranium. The radio elements of these granites are incorporated in their accessory minerals such as zircon, xenotime and allanite.

REFERENCES

Abdel-Karim, A.M. (1996): Petrogenesis of Late Precambrian younger granites from southwest Sinai, Egypt. J. Min. Petr. Econ. Geol. 91, 185-195.

Abu El Leil, I., (1980): Geology, petrography and geochemistry of some granitic rocks in the northern part of the basement complex, Egypt. Ph. D. Thesis, Al Azhar Univ., Egypt.

Azzaz, S. A. (1993): Petrogenesis of granitoid rocks of Wadi Baba area, southern Sinai, Egypt. J KAU: Earth Sci., 6, 79-98.

Bishr, A. H. A., 2003: Geology, radioactivity and mineralogical studies of some granitic plutons in Wadi Um Hamd environs, southwestern Sinai, Egypt. M. Sc. Thesis, Mans. Univ., 132 p.

El Bouseily, A.M and El-Sokkary, A.A., 1975: The relationship between Rb, Sr and Ba in granitic rocks. Chem. Geol., V.16, P174-189.

El Galy, M. M. (2003): Review article in application of equilibrium-disequilibrium phenomena of the U-Th decay series in exploration for uranium ore deposits. Nuclear Materials Authority.

El Husseiny, M.O., (2008): Geochemistry and Rare Earth elements in younger granitic rocks of Wadi El Sahu-Wadi El Seih area, southwest Sinai, Egypt. Annals Geol. Surv. Egypt, V. XXX, 2008, pp 65-82.

Gabr, M. M. (2005): Zircon typology and uranium mineralization of some younger granite plutons, south western Sinai, Egypt. Ph. D. Thesis, Suez Canal Univ. Egypt. 156 p.

Hassan, I. H. I. (1997): Geology and radioactivity of the basement rocks of Wadi El-Shallal area, Southwestern Sinai, Egypt. M.Sc. Thesis. Ain Shams Univ. Cairo, Egypt.120 p.

Hussein A. H. (1978): Lecture Course in Nuclear Geology, 101p., NMA, Egypt.

Loiselle, M. C. and Wones, D. R. (1979): Characteristics and origins of anoroginic granite, Geol. Soc. Am; Abstract with program 11:468.

Maniar, P. D. and Piccoli, P. M., (1989): Tectonic discrimination of granitoids. Geol. Soc. Am. Bull. V. 101, pp. 635-643.

Pearce. J. A., Harris, N. B. W. and Tindle, A. G., (1984): Trace element discrimination diagrams for the tectonic interpretation of granitic rocks. J. Petro. Vol. 25 (4), pp. 956-983.

Petro, W.L.; Vogel, T.A. and Wilband, J.T., 1979: Major element chemistry of plutonic rock suites from compressional and extensional plate boundaries. Chem. Geol., V.26, pp: 217-235.

Sabet, A. H., Bessonenko, V. V. and Bykov, B. A., (1976): The intrusive complexes of the Central Eastern Desert of Egypt. Annals Geol. Surv. Egypt, 6: 53-73.

Shand, S.J., 1951: Eruptive rocks. John-Wiley, New York, 4th edition, 360p.

Shelley, D., (1993): Igneous and metamorphic rocks under the microscope. Champan and Hall. London. Glasgow. New York. 445 p.

Sherif, H.M. and Ragab, A. A. (2004): Geology, geochemistry and radioactivity of Wadi Abu El Tiyour area, southwestern Sinai, Egypt. Proceedings of the sixth International Conference on Geochemistry, Alexandria, Egypt. Vol. 1-p. 577-606 pp.

Sherif, H.M.Y., (1998): Geology and uranium potentiality of Wadi Seih area,southwest Sinai ,Egypt. Ph.D. Thesis,Cairo Univ. Geza,Egypt.229 p.

Streckeisen, A., (1976): To each plutonic rocks its proper name. Earth Science Reviews, Vol.12, P. 1-33.

Tarney, J. (1977): Petrology, mineralogy and geochemistry of the Falkland Plateau basement rocks, site 300, Deep Sea Drilling Proect.Int.Rep. Deep Sea Drilling Project 36,893-921.

Weaver B. and Tarney J. (1984): Empirical approach to estimating the composition of the continental crust. Nature, 310, 575-57.

Werner, C.D. (1987): Saxonian granulites-igneous or lithigneous: A contribution to the geochemical diagnosis of the original rocks in high temperature complexes. In: Gerstenberger, H.(ed): contribution to the geology of the Saxonian massif (Sashsisches Granulitegebirge), Z ft- Mitteilungen,133,221-250.
Wright, J. B., (1969): A simple alkalinity ratio and its application to question nonorogenic granite gneisses. Geol. Mag., 106: 370-384.

Cite this Article: El Mezayen AM, Abu Bakr MA, Sherif HMY, El Nahas HA and Ali HH (2016). Geology and Radioactivity of the Basement Rocks of Wadi El-Sahu Area, Southwestern Sinai, Egypt. Greener Journal of Geology and Earth Sciences, 4(1): 001-022, http://doi.org/10.15580/GJGES.2016.1.021716041